NEW DIFFRACTION DATA

Crystal structure of anthraquinone-2-carboxylic acid, $C_{15}H_8O_4$

Tawnee M. Ens,[1] James A. Kaduk [ORCID],[2,3,a] Anja Dosen [ORCID],[4] and Thomas N. Blanton [ORCID][4]

[1]North Central College, 131 S. Loomis St., Naperville, IL 60540, USA
[2]Illinois Institute of Technology, 3101 S. Dearborn St., Chicago, IL 60616, USA
[3]North Central College, 131 S. Loomis St., Naperville, IL 60540, USA
[4]ICDD, 12 Campus Blvd., Newtown Square, PA 19073-3273, USA

The crystal structure of anthraquinone-2-carboxylic acid has been solved and refined using synchrotron X-ray powder diffraction data, and optimized using density functional theory techniques. Anthraquinone-2-carboxylic acid crystallizes in space group P-1 (#2) with $a = 3.7942(2)$, $b = 13.266(5)$, $c = 22.835(15)$ Å, $\alpha = 73.355(30)$, $\beta = 89.486(6)$, $\gamma = 86.061(1)°$, $V = 1098.50(7)$ Å^3, and $Z = 4$. The crystal structure contains two independent molecules of anthraquinone-2-carboxylic acid. Although the expected hydrogen-bonded dimers are present, the dimers are not centrosymmetric. The dimer contains one molecule of each planar low-energy conformation. The crystal structure consists of a herringbone array of centrosymmetric pairs of molecules parallel to the bc-plane. The molecules stack along the short a-axis. The powder pattern has been submitted to ICDD® for inclusion in the Powder Diffraction File™ (PDF®).

[doi:10.1017/S0885715624000046]

I. INTRODUCTION

Anthraquinone-2-carboxylic acid (AQCA) is in the class of polyphenols that possess anti-inflammatory qualities. AQCA is abundant in *Tabebuia* bignoniaceae (trumpet tree) tree bark and has been found to inhibit the COX-2 (cyclooxygenase) enzyme (Ma et al., 2017). Its anti-inflammatory properties have been investigated by Park et al. (2016). The systematic name (CAS Registry Number 117-78-2) is 9,10-dioxoanthracene-2-carboxylic acid. A two-dimensional molecular structure is shown in Figure 1.

X-ray powder diffraction patterns of AQCA and its methanol solvate have been reported by Tsai et al. (1993), and a variety of other physical properties were determined. A connectivity search in the Cambridge Structural Database (Groom et al., 2016) yielded crystal structures of a DMSO adduct (Gruber et al., 2010; TAJGIW) and two clathrates (Kobayashi et al., 2008; WIXVOP and WIXVUV), but no structures of pure AQCA.

This work was carried out as part of a project (Kaduk et al., 2014) to determine the crystal structures of large-volume commercial pharmaceuticals, and include high-quality powder diffraction data for them in the Powder Diffraction File (Gates-Rector and Blanton, 2019).

II. EXPERIMENTAL

AQCA was a commercial reagent, purchased from TargetMol (Batch #119182), and was used as-received. The yellow powder was packed into a 1.5-mm diameter Kapton capillary, and rotated during the measurement at ~50 Hz. The powder pattern was measured at 295 K at beam line 11-BM (Antao et al., 2008; Lee et al., 2008; Wang et al., 2008) of the Advanced Photon Source at Argonne National Laboratory using a wavelength of 0.458153(2) Å from 0.5° to 50° 2θ with a step size of 0.001° and a counting time of 0.1 s/step. The high-resolution powder diffraction data were collected using twelve silicon crystal analyzers that allow for high angular resolution, high precision, and accurate peak positions. A mixture of silicon (NIST SRM 640c) and
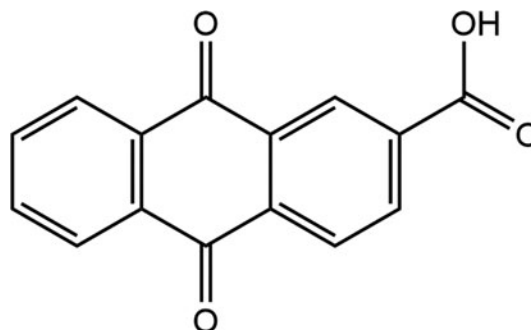

Figure 1. The two-dimensional structure of anthraquinone-2-carboxylic acid.

a)Author to whom correspondence should be addressed. Electronic mail:
kaduk@polycrystallography.com

alumina (NIST SRM 676a) standards (ratio Al_2O_3:Si = 2:1 by weight) was used to calibrate the instrument and refine the monochromatic wavelength used in the experiment.

The pattern was indexed using DICVOL14 (Louër and Boultif, 2014) on a primitive monoclinic unit cell with $a = 22.70667$, $b = 3.73900$, $c = 26.39351$ Å, $\beta = 106.563°$, $V = 2148.35$ Å^3, and $Z = 8$. Up to three unindexed lines were permitted. Analysis of the systematic absences using EXPO2014 (Altomare et al., 2013) suggested the space group $P2_1$, so there were four molecules in the asymmetric unit. A reduced cell search of the Cambridge Structural Database (Groom et al., 2016) yielded no hits.

The AQCA molecule was downloaded from PubChem (Kim et al., 2023) as Conformer3D_CID_67030.sdf, and converted to a *.mol2 file using Mercury (Macrae et al., 2020). The crystal structure was solved using Monte Carlo simulated annealing techniques as implemented in EXPO2014 (Altomare et al., 2013). The best two of the ten solutions were similar. The remaining solutions contained close intermolecular contacts, so the best solution was selected for initial refinement.

After initial refinement, the carboxylic acid group of one of the four molecules made close intermolecular contacts with aromatic C–H groups, and was not in a position to form hydrogen bonds. Accordingly, the molecule was "flipped" 180° using Materials Studio (Dassault Systèmes, 2022) to an orientation more suitable for hydrogen bonding, and the structure was re-refined. Analysis of potential hydrogen bonds (using the O⋯O distances) made the approximate positions of the carboxylic acid protons clear.

Rietveld refinement was carried out using GSAS-II (Toby and Von Dreele, 2013). Only the $0.9°$–$25.0°\theta$ portion of the pattern was included in the refinement ($d_{min} = 1.058$ Å). All of the carbon, aromatic hydrogen atoms, and quinone oxygen atoms were modeled using a $C_{15}H_8O_2$ rigid body, derived from optimization of the AQCA structure from PubChem using Spartan '20 (Wavefunction, 2022), and removing the 2O and H atoms of the carboxylic acid group. The group

was saved as an *.xyz file, and imported into GSAS-II as a vector rigid body. Only the O atoms of the carboxylic acid groups were refined independently, subject to C–O bond restraints of 1.27(5) Å, and bond angle restraints of O–C–O = 125(3) and C–C–O = 117.5(30)°, to permit rotation of the carboxylic acid groups. The active H atoms were fixed based on the results of the density functional theory (DFT) calculation. An independent U_{iso} was refined for each of the four rigid bodies. The U_{iso} of the two O atoms in each carboxyl group were constrained to a common value. A preferred orientation model was included in the refinement as sixth-order spherical harmonics. The peak profiles were described using the generalized microstrain model (Stephens, 1999). The background was modeled using a six-term shifted Chebyshev polynomial, and a peak at $6.17°$ 2θ to model the scattering from the Kapton capillary and any amorphous component.

The final refinement (begun from the DFT-optimized structure) of seventy-eight variables using 24,139 observations and twenty restraints yielded the residuals $R_{wp} = 0.19333$ and GOF = 4.10. The largest peak (0.139 Å from C5) and hole (1.964 Å from C94) in the difference Fourier map were 0.67(16) and $-0.68(16)$ eÅ^{-3}, respectively. The largest errors in the difference plot (Figure 2) were in peak intensities, and the refinement overall was unsatisfactory. There were unindexed peaks. The Certificate of Analysis indicates 99.83% purity, so they may represent the trace presence of an additional polymorph.

Tsai et al. (1993) indicated that AQCA could be recrystallized by sublimation, so a second sample was purchased (Sigma–Aldrich 1003514978) and an aliquot was recrystallized by placing as-received powder in a beaker and heating it on a hot plate, while covering the beaker with a watch glass. Long needles were produced (Figure 3). A portion of the needles was ground in a mortar and pestle, and packed into a 0.3-mm diameter glass capillary. The X-ray powder diffraction pattern was measured on a PANalytical Empyrean diffractometer equipped with an incident-beam focusing mirror
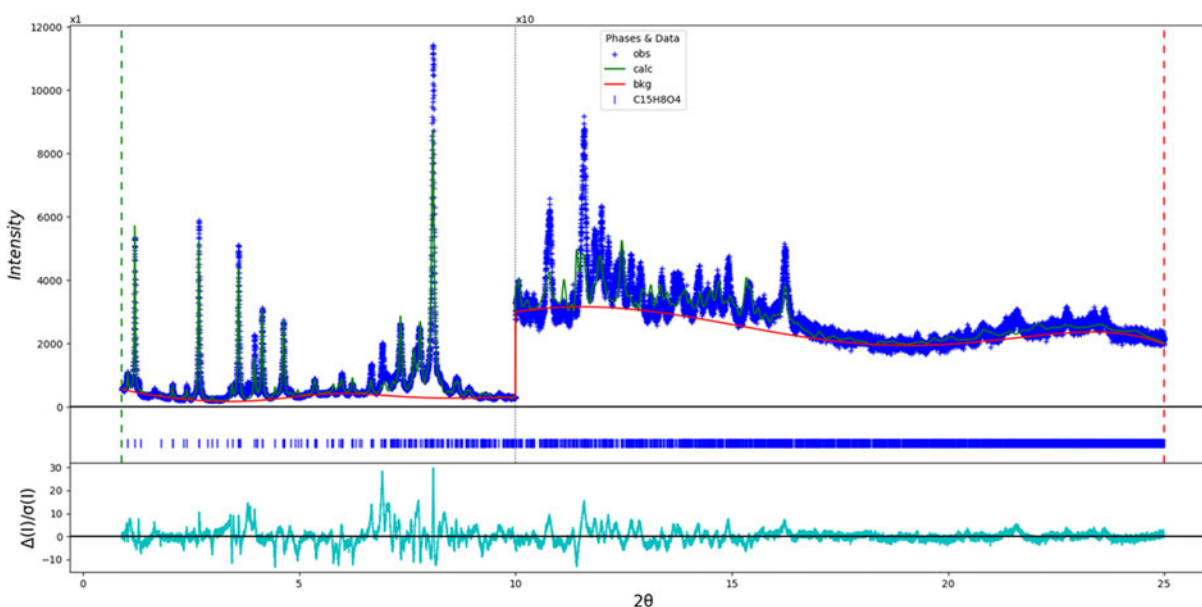

Figure 2. The Rietveld plot for the incorrect refinement of anthraquinone-2-carboxylic acid. The blue crosses represent the observed data points, and the green line is the calculated pattern. The cyan curve is the normalized error plot, and the red line is the background curve. The vertical scale has been multiplied by a factor of 10× for $2\theta > 10.0°$.
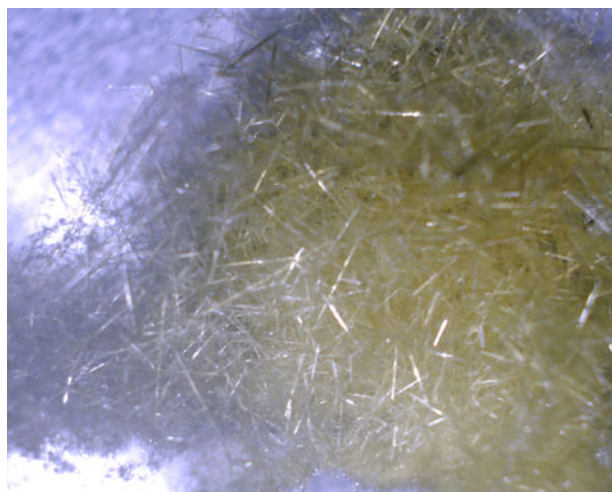
Figure 3. An optical micrograph of the needles obtained by recrystallizing anthraquinone-2-carboxylic acid by sublimation.

and an X'Celerator detector. The pattern (1°–50° 2θ, 0.0083556° steps, 4.0 s/step, 1/4° divergence slit, 0.02 radian Soller slits) was measured using Mo K_α radiation.

Several peaks that were present in the original synchrotron pattern were not observed in the pattern of the recrystallized sample (Figure 4). The laboratory pattern was indexed using N-TREOR (Altomare et al., 2013) on a primitive triclinic cell having $a = 3.7985$, $b = 12.2241$, $c = 22.8641$ Å, $\alpha = 73.485$, $\beta = 89.934$, $\gamma = 86.453°$, $V = 1098.7$ Å^3, and $Z = 4$. A reduced cell search in the Cambridge Structural Database (Groom et al., 2016) yielded no hits.

The structure was solved using the triclinic cell and the synchrotron data with EXPO2014 (Altomare et al., 2013), using two molecules as fragments. A bump penalty and (100) preferred orientation were included.

Separate Rietveld refinements were carried out with GSAS-II (Toby and Von Dreele, 2013) using the synchrotron and laboratory data (different samples). All non-H bond distances and angles were subjected to restraints, based on a

Mercury/Mogul Geometry Check (Bruno et al., 2004; Sykes et al., 2011). The Mogul average and standard deviation for each quantity were used as the restraint parameters. The anthraquinone ring systems and the carboxyl groups were restrained to be planar. The hydrogen atoms were included in calculated positions, which were recalculated during the refinement using Materials Studio (Dassault, 2022). The U_{iso} of the heavy atoms were grouped by chemical similarity. The U_{iso} for the H atoms were fixed at 1.3× the U_{iso} of the heavy atoms to which they are attached. The peak profiles were described using the generalized microstrain model. The refinements yielded the residuals included in Table I. The final Rietveld plots are shown in Figure 5.

The structure of AQCA was optimized (fixed experimental unit cell) with density functional techniques using VASP (Kresse and Furthmüller, 1996) through the MedeA graphical interface (Materials Design, 2016). The calculation was carried out on 16 2.4 GHz processors (each with 4 Gb RAM) of a 64-processor HP Proliant DL580 Generation 7 Linux cluster at North Central College. The calculation used the GGA-PBE functional, a plane wave cutoff energy of 400.0 eV, and a k-point spacing of 0.5 Å^{-1} leading to a 4 × 1 × 1 mesh, and took ~6.2 h. Single-point density functional calculations (fixed experimental cell) and population analysis were carried out using CRYSTAL23 (Erba et al., 2023). The basis sets for the H, C, and O atoms in the calculation were those of Gatti et al. (1994). The calculations were run on a 3.5 GHz PC using 14 k-points and the B3LYP functional, and took ~2.6 h. VASP indicated that this compound is a semiconductor, with a band gap of 1.745 eV.

III. RESULTS AND DISCUSSION

The powder pattern of this study is similar enough to that reported by Tsai et al. (1993; Figure 6) to conclude that they probably represent the same material, but there are differences, so the conclusion is not certain. The material used by Tsai et al. may contain an additional polymorph. Our material is probably representative of that used in commerce.
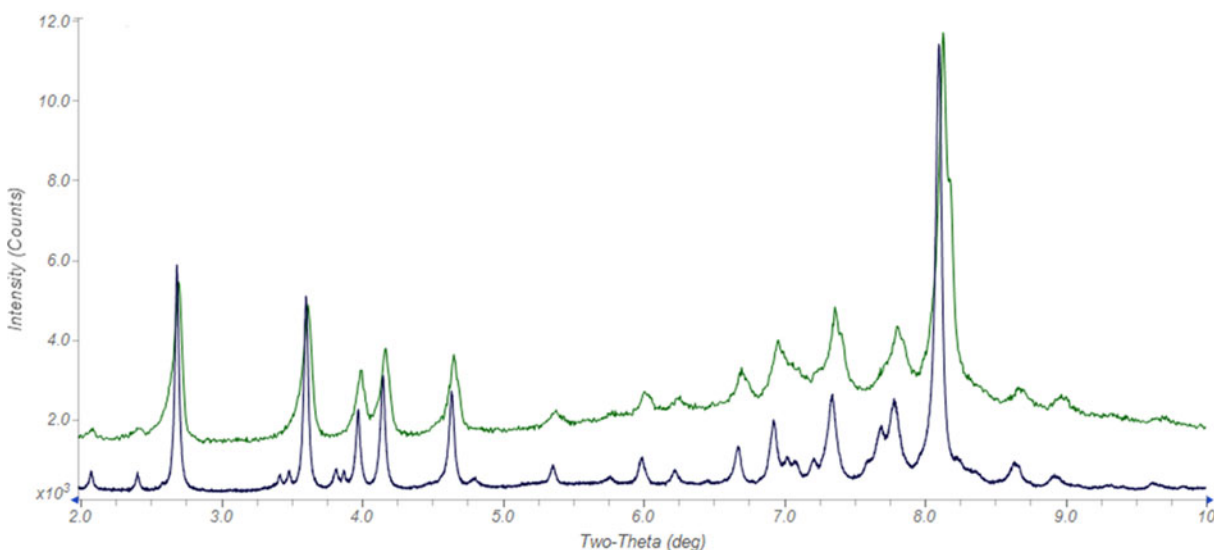

Figure 4. Comparison of the synchrotron pattern of anthraquinone-2-carboxylic acid (black) to that of the recrystallized material (green). The laboratory pattern (measured using Mo K_α radiation) was converted to the synchrotron wavelength of 0.458153(2) Å using JADE Pro (MDI, 2023). Image generated using JADE Pro (MDI, 2023).

TABLE I. Summary of refinement residuals for the different data sets of anthraquinone-2-carboxylic acid.

Data	Synchrotron	Laboratory
Range, 2θ	1.1–25.0	1.2–30.0
d_{min}, Å	1.058	1.370
R_{wp}	0.1295	0.0444
GOF	2.76	1.94
% χ^2 from restraints	8.1	16.3
# variables	141	139
# observations	23,939	3,447
# restraints	108	108
Texture index	1.061	1.071

The crystal structure contains two independent molecules of AQCA. The molecules with atom numbering are illustrated in Figure 7. Although the expected hydrogen-bonded dimers are present, the dimers are not centrosymmetric. The dimer contains one molecule of each planar low-energy conformation.

The root-mean-square (rms) Cartesian displacements of the non-H atoms in the Rietveld-refined and VASP-optimized molecules are 0.327 and 0.092 Å for molecule 1 (lower atom numbers) and molecule 2. The agreements are within the normal range for correct structures (van de Streek and Neumann, 2014). The largest differences are in the orientation of the carboxylic acid group in molecule 1. The rms difference in the absolute positions in the unit cell is 0.454 Å (Figure 8).
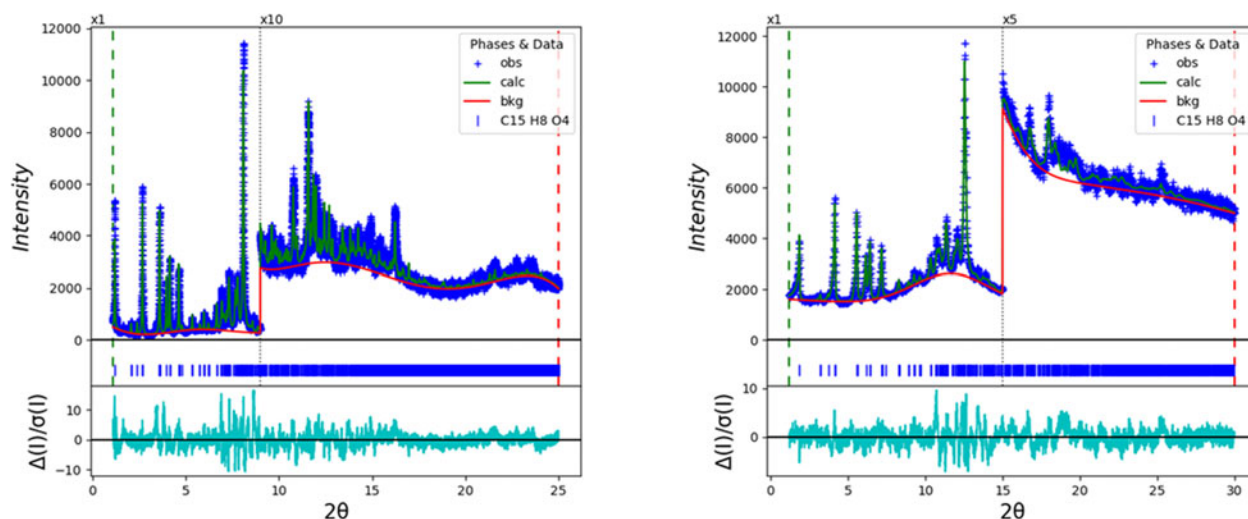

Figure 5. Final Rietveld plots for the refinements of anthraquinone-2-carboxylic acid using synchrotron (left) and laboratory (right) data. The blue crosses represent the observed data points, and the green line is the calculated pattern. The cyan curve is the normalized error plot, and the red line is the background curve.
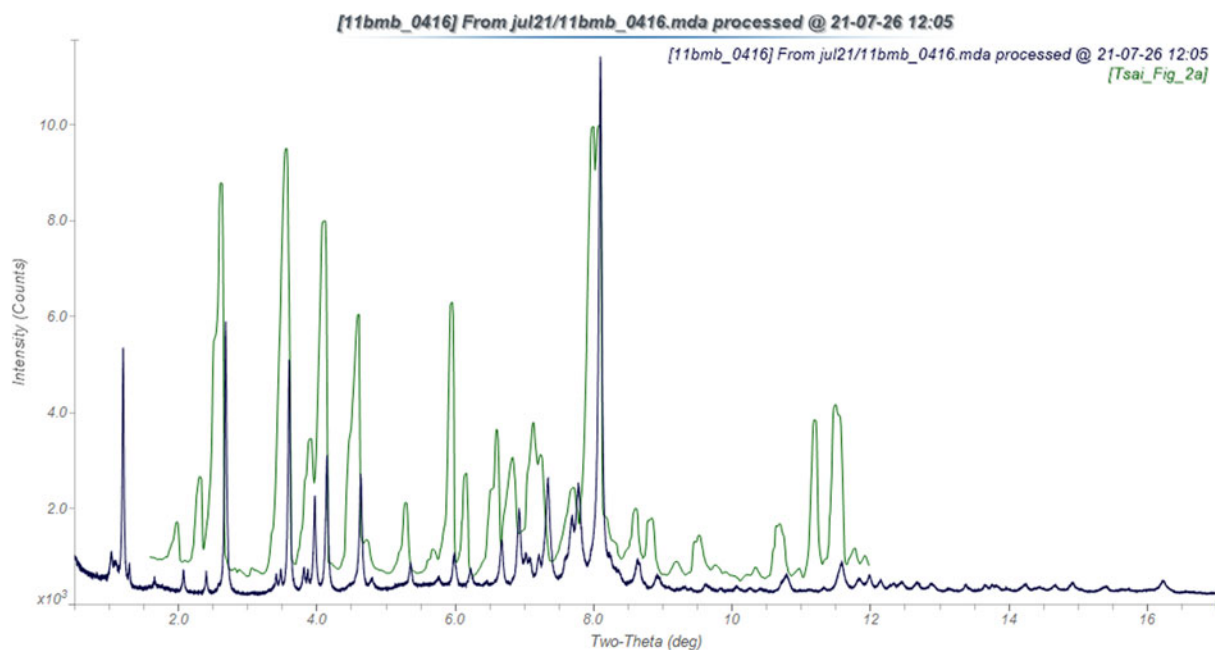

Figure 6. Comparison of the synchrotron pattern of anthraquinone-2-carboxylic acid (black) to that reported by Tsai et al. (1993; green). The literature pattern (measured using Cu K$_\alpha$ radiation) was digitized using UN-SCAN-IT (Silk Scientific, 2013) and converted to the synchrotron wavelength of 0.458153(2) Å using JADE Pro (MDI, 2023). Image generated using JADE Pro (MDI, 2023).
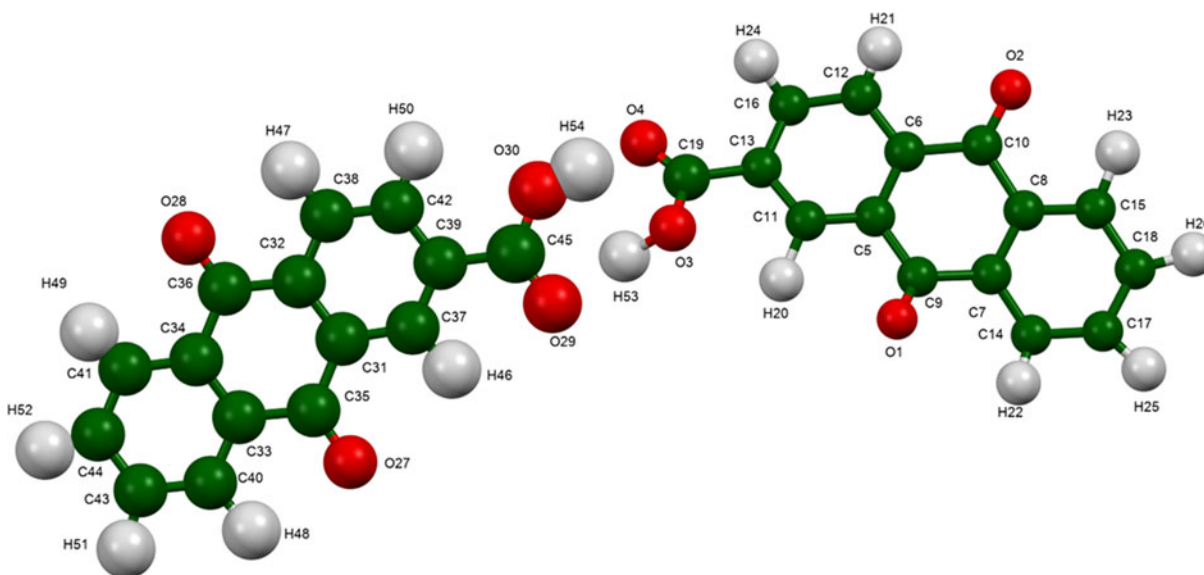
Figure 7. The asymmetric unit of anthraquinone-2-carboxylic acid, with the atom numbering. The atoms are represented by 50% probability spheroids. Image generated using Mercury (Macrae et al., 2020).
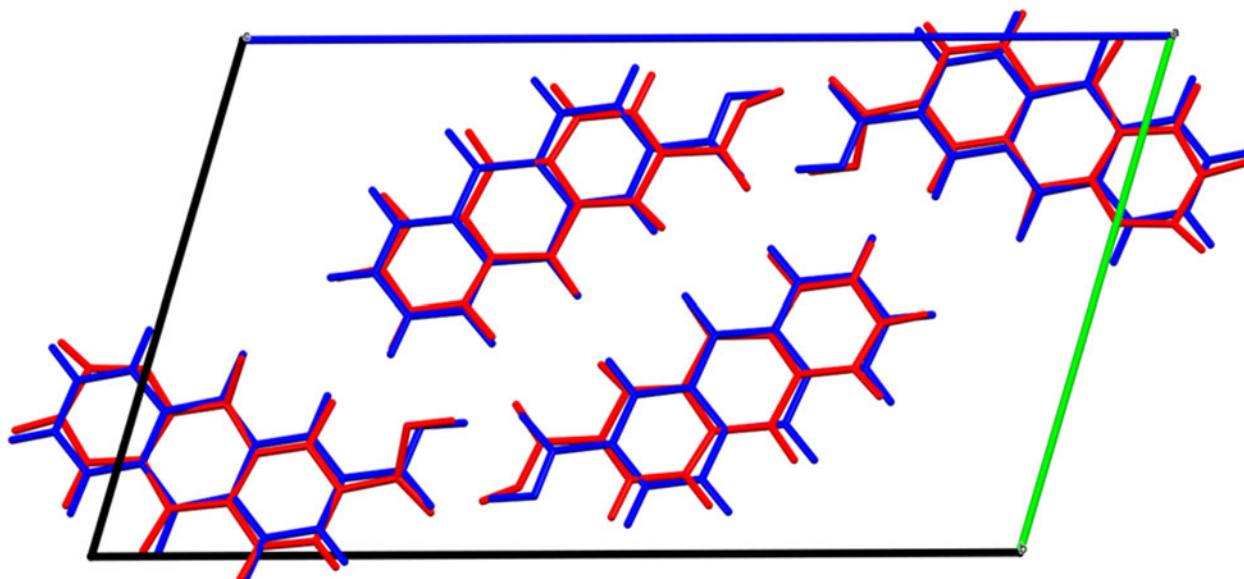

Figure 8. Comparison of the Rietveld-refined (red) and VASP-optimized (blue) structures of anthraquinone-2-carboxylic acid. Image generated using Mercury (Macrae et al., 2020).

The relatively limited range of data and the relatively broad peaks limit the accuracy which can be achieved. The remainder of this discussion will emphasize the VASP-optimized structure.

The crystal structure (Figure 9) consists of a herringbone array of centrosymmetric pairs of molecules parallel to the *bc*-plane, or alternatively arrangement of non-centrosymmetric hydrogen-bonded dimers along the *c*-axis. The molecules stack along the short *a*-axis. The mean planes of the anthraquinone ring systems are approximately –5, –5, 8 and 4, 6, –1. The Mercury Aromatics Analyser indicated strong interactions along the *a*-axis, with a distance of 3.79 Å.

All of the bond distances, bond angles, and torsion angles fall within the normal ranges indicated by a Mercury Mogul Geometry check (Macrae et al., 2020). Quantum chemical geometry optimization of the isolated molecules (DFT/ B3LYP/6-31G*/water) using Spartan '20 (Wavefunction, 2022) indicated the two conformations are essentially identical in energy, as expected (Kaduk et al., 1998).

Analysis of the contributions to the total crystal energy of the structure using the Forcite module of Materials Studio (Dassault Systèmes, 2022) suggests that bond distortion terms dominate the intramolecular deformation energy. The intermolecular energy is dominated by electrostatic attractions, which in this force field analysis also include hydrogen bonds. The hydrogen bonds are better analyzed using the results of the DFT calculation.

Hydrogen bonds (Table II) are prominent in the crystal structure. The two independent molecules are linked into dimers through strong O–H⋯O hydrogen bonds. The energies
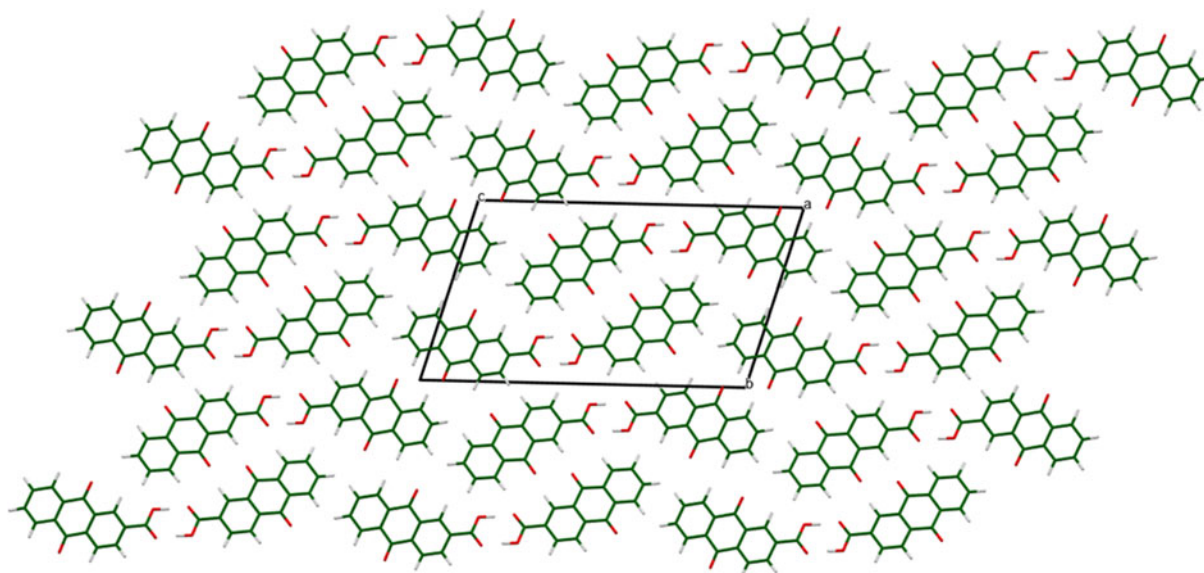
Figure 9. The crystal structure of anthraquinone-2-carboxylic acid, viewed down the *a*-axis. Image generated using Mercury (Macrae et al., 2020).

TABLE II. Hydrogen bonds (CRYSTAL23) in anthraquinone-2-carboxylic acid.

H-Bond	D–H, Å	H···A, Å	D···A, Å	D–H···A,°	Overlap, *e*	*E*, kcal/mol
O30–H54···O4	1.042	1.523	2.563	176.0	0.081	15.6
O3–H53···O29	1.057	1.449	2.503	174.2	0.087	16.1
C43–H51···O3	1.089	2.439	3.295	134.5	0.011	
C40–H48···O27	1.090	2.451[a]	2.800	96.9	0.014	
C37–H46···O27	1.090	2.649	3.632	149.7	0.011	
C15–H23···O2	1.088	2.287	3.190	139.0	0.015	
C15–H23···O2	1.088	2.479[a]	2.841	96.0	0.010	
C12–H21···O2	1.089	2.457[a]	2.787	95.8	0.015	
C11–H20···O1	1.089	2.464[a]	2.804	96.5	0.018	

[a]Intramolecular charge.

of these O–H···O hydrogen bonds were estimated using a correlation derived from the results of Rammohan and Kaduk (2018). Several C–H···O bonds, both intra- and intermolecular, also contribute to the lattice energy.

The Bravais–Friedel–Donnay–Harker (Bravais, 1866; Friedel, 1907; Donnay and Harker, 1937) model suggests that we might expect needle morphology for AQCA, with ⟨100⟩ as the long axis, and an aspect ratio of approximately 6:1 (Figure 10). This morphology is consistent with that of the recrystallized sample. A second-order spherical harmonic model for preferred orientation was included in the refinements. As noted in Table I, the texture indices were not
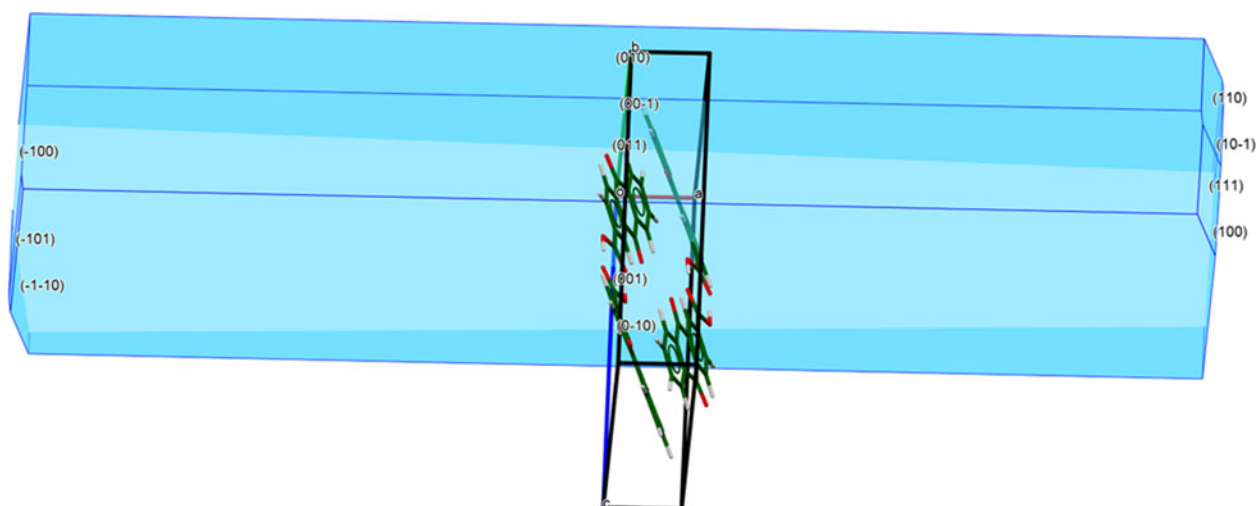

Figure 10. The Bravais–Friedel–Donnay–Harker morphology of anthraquinone-2-carboxylic acid, predicted by Mercury. Image generated using Mercury (Macrae et al., 2020).

especially high, showing that preferred orientation was minor in these rotated capillary specimens.

IV. DEPOSITED DATA

The powder pattern of AQCA from this synchrotron data set has been submitted to ICDD for inclusion in the Powder Diffraction File. The Crystallographic Information Framework (CIF) files containing the results of the Rietveld refinement (including the raw data) and the DFT geometry optimization were deposited with the ICDD. The data can be requested at pdj@icdd.com.

ACKNOWLEDGEMENTS

CONFLICTS OF INTEREST

The authors have no conflicts of interest to declare.

REFERENES

Altomare, A., C. Cuocci, C. Giacovazzo, A. Moliterni, R. Rizzi, N. Corriero, and A. Falcicchio. 2013. "EXPO2013: A Kit of Tools for Phasing Crystal Structures from Powder Data." *Journal of Applied Crystallography* 46: 1231–5.

Antao, S. M., I. Hassan, J. Wang, P. L. Lee, and B. H. Toby. 2008. "State-of-the-Art High-Resolution Powder X-Ray Diffraction (HRPXRD) Illustrated with Rietveld Refinement of Quartz, Sodalite, Tremolite, and Meionite." *Canadian Mineralogist* 46: 1501–9.

Bravais, A. 1866. *Etudes Cristallographiques*. Paris, Gauthier Villars.

Bruno, I. J., J. C. Cole, M. Kessler, J. Luo, W. D. S. Motherwell, L. H. Purkis, B. R. Smith, R. Taylor, R. I. Cooper, S. E. Harris, and A. G. Orpen. 2004. "Retrieval of Crystallographically-Derived Molecular Geometry Information." *Journal of Chemical Information and Computer Sciences* 44: 2133–44.

Dassault Systèmes. 2022. *BIOVIA Materials Studio 2023*. San Diego, CA, BIOVIA.

Donnay, J. D. H., and D. Harker. 1937. "A New Law of Crystal Morphology Extending the Law of Bravais." *American Mineralogist* 22: 446–66.

Erba, A., J. K. Desmaris, S. Casassa, B. Civalleri, L. Donà, I. J. Bush, B. Searle, L. Maschio, L.-E. Daga, A. Cossard, C. Ribaldone, E. Ascrizzi, N. L. Marana, J.-P. Flament, and B. Kirtman. 2023. "CRYSTAL23: A Program for Computational Solid State Physics and Chemistry." *Journal of Chemical Theory and Computation* 19: 6891–932. doi:10.1021/acs.jctc.2c00958.

Friedel, G. 1907. "Etudes sur la loi de Bravais." *Bulletin de la Société Française de Minéralogie* 30: 326–455.

Gates-Rector, S., and T. N. Blanton. 2019. "The Powder Diffraction File: A Quality Materials Characterization Database." *Powder Diffraction* 39: 352–60.

Gatti, C., V. R. Saunders, and C. Roetti. 1994. "Crystal-Field Effects on the Topological Properties of the Electron-Density in Molecular Crystals - the Case of Urea." *Journal of Chemical Physics* 101: 10686–96.

Groom, C. R., I. J. Bruno, M. P. Lightfoot, and S. C. Ward. 2016. "The Cambridge Structural Database." *Acta Crystallographica Section B: Structural Science, Crystal Engineering and Materials* 72: 171–9.

Gruber, T., S. F. Helas, W. Seichter, and E. Weber. 2010. "X-Ray Crystal Structures of Two Solvent Complexes Involving Positionally Isomeric 9, 10-Anthraquinonecarboxylic Acids and DMSO." *Structural Chemistry* 21: 1079–83. doi:10.1007/s11224-010-9648-0.

Kaduk, J. A., J. T. Golab, and F. J. J. Leusen. 1998. "The Crystal Structure of Trimellitic Anhydride and Two of Its Solvates." *Crystal Engineering* 1: 277–90.

Kaduk, J. A., C. E. Crowder, K. Zhong, T. G. Fawcett, and M. R. Suchomel. 2014. "Crystal Structure of Atomoxetine Hydrochloride (Strattera), $C_{17}H_{22}NOCl$." *Powder Diffraction* 29: 269–73.

Kim, S., J. Chen, T. Cheng, A. Gindulyte, J. He, S. He, Q. Li, B. A. Shoemaker, P. A. Thiessen, B. Yu, L. Zaslavsky, J. Zhang, and E. E. Bolton. 2023. "Pubchem 2023 Update." *Nucleic Acids Research* 51 (D1): D1373–80. doi:10.1093/nar/gkac956.

Kobayashi, Y., K. Kodama, and K. Saigo. 2008. "Enantioselective inclusion of chiral alkyl aryl sulfoxides in a supramolecular helical channel consisting of an enantiopure 1, 2-amino alcohol and an achiral carboxylic acid." *Tetrahedron: Asymmetry* 19: 295–301. doi:10.1016/j.tetasy.2007.11.041.

Kresse, G., and J. Furthmüller. 1996. "Efficiency of Ab-Initio Total Energy Calculations for Metals and Semiconductors Using a Plane-Wave Basis Set." *Computational Materials Science* 6: 15–50.

Lee, P. L., D. Shu, M. Ramanathan, C. Preissner, J. Wang, M. A. Beno, R. B. Von Dreele, L. Ribaud, C. Kurtz, S. M. Antao, X. Jiao, and B. H. Toby. 2008. "A Twelve-Analyzer Detector System for High-Resolution Powder Diffraction." *Journal of Synchrotron Radiation* 15: 427–32.

Louër, D., and A. Boultif. 2014. "Some Further Considerations in Powder Diffraction Pattern Indexing with the Dichotomy Method." *Powder Diffraction* 29: S7–12.

Ma, S., K. Yada, H. Lee, Y. Fukuda, A. Iida, and K. Suzuki. 2017. "Taheebo polyphenols attenuate free fatty acid-induced inflammation in murine and human macrophage cell lines as inhibitor of cyclooxygenase-2." *Frontiers in Nutrition* 4: 63. doi:10.3389/fnut.2017.00063. Erratum in: Frontiers in Nutrition 2018: 5: 2.

Macrae, C. F., I. Sovago, S. J. Cottrell, P. T. A. Galek, P. McCabe, E. Pidcock, M. Platings, G. P. Shields, J. S. Stevens, M. Towler, and P. A. Wood. 2020. "*Mercury 4.0*: From Visualization to Design and Prediction." *Journal of Applied Crystallography* 53: 226–35.

Materials Design. 2016. *MedeA 2.20.4*. Angel Fire, NM, Materials Design Inc.

MDI. 2023. *JADE Pro Version 8.3*. Livermore, CA, Materials Data.

Park, J. G., S. C. Kim, Y. H. Kim, W. S. Yang, Y. Kim, S. Hong, K.-H. Kim, B. C. Yoo, S. H. Kim, J. H. Kim, and J. Y. Cho. 2016. "Anti-Inflammatory and Antinociceptive Activities of Anthraquinone-2-Carboxylic Acid." *Mediators of Inflammation* 2016: 1903849.

Rammohan, A., and J. A. Kaduk. 2018. "Crystal Structures of Alkali Metal (Group 1) Citrate Salts." *Acta Crystallographica Section B: Crystal Engineering and Materials* 74, 239–52. doi:10.1107/S2052520618002330.

Silk Scientific. 2013. *UN-SCAN-IT 7.0*. Orem, UT, Silk Scientific Corporation.

Stephens, P. W. 1999. "Phenomenological Model of Anisotropic Peak Broadening in Powder Diffraction." *Journal of Applied Crystallography* 32: 281–9.

Sykes, R. A., P. McCabe, F. H. Allen, G. M. Battle, I. J. Bruno, and P. A. Wood. 2011. "New Software for Statistical Analysis of Cambridge Structural Database Data." *Journal of Applied Crystallography* 44: 882–6.

Toby, B. H., and R. B. Von Dreele. 2013. "GSAS II: The Genesis of a Modern Open Source All Purpose Crystallography Software Package." *Journal of Applied Crystallography* 46: 544–9.

Tsai, S.-Y., S.-C. Kuo, and S.-Y. Lin. 1993. "Physicochemical Characterization of 9,10-Anthraquinone 2-Carboxylic Acid." *Journal of Pharmaceutical Sciences* 82: 1250–4.

van de Streek, J., and M. A. Neumann. 2014. "Validation of Molecular Crystal Structures from Powder Diffraction Data with Dispersion-Corrected Density Functional Theory (DFT-D)." *Acta Crystallographica Section B: Structural Science, Crystal Engineering and Materials* 70: 1020–32.

Wang, J., B. H. Toby, P. L. Lee, L. Ribaud, S. M. Antao, C. Kurtz, M. Ramanathan, R. B. Von Dreele, and M. A. Beno. 2008. "A Dedicated Powder Diffraction Beamline at the Advanced Photon Source: Commissioning and Early Operational Results." *Review of Scientific Instruments* 79: 085105.

Wavefunction, Inc. 2022. *Spartan '20. V. 1.1.4*. Irvine, CA: Wavefunction Inc.